Multiple magnetic transitions, anomalous Hall effect and tunable surface states in $Mn(Bi_{1-x}Sb_x)_4Te_7$

Chandan De,[1,2,3] Keisuke Fukutani,[1,4] Junho Seo,[1,5] Roland Stania,[1] Koichiro Yaji,[6,7] Kenta Kuroda,[6,8,5] Jun Sung Kim,[1,5] Han Woong Yeom,[1] and Sang-Wook Cheong[2,9,*]

[1] *Center for Artificial Low Dimensional Electronic Systems, Institute for Basic Science (IBS), Pohang 37673, Korea*

[2] *Laboratory of Pohang Emergent Materials, Pohang Accelerator Laboratory, Pohang 37673, Korea*

[3] *Current affiliation: Quantum Materials Science Unit, Okinawa Institute of Science and Technology (OIST), Okinawa 904-0495, Japan*

[4] *Current affiliation: Institute for Molecular Science, Okazaki, Aichi 444-8585, Japan*

[5] *Department of Physics, Pohang University of Science and Technology (POSTECH), Pohang 37673, Korea*

[6] *Institute for Solid State Physics, University of Tokyo, Kashiwa 277-8581, Japan*

[7] *Current afilliation: Research Center for Advanced Measurement and Characterization, National Institute for Materials Science, Ibaraki 305-0047, Japan*

[8] *Current afilliation: Graduate School of Advanced Science and Engineering, Hiroshima University, Higashi-Hiroshima, Hiroshima 739-8526, Japan*

[9] *Keck Center for Quantum Magnetism and Department of Physics & Astronomy, Rutgers University, 136 Frelinghuysen Road, Piscataway, NJ 08854, USA*

(Dated: Oct 2024)

Abstract

Anomalous Hall effect due to an intricsic magnetic ordering combined with topological electronic states is at the forefront of recent study in the condensed matter physics. The seminal compound $MnBi_2Te_4$ has fueled an enormous interest for the study of various exotic quantum phenomena such as axion insulator state, chern insulator state and quantum anomalous Hall effect on this materials as well as its hetero-structural cousins $(MnBi_2Te_4)(Bi_2Te_3)n$. Despite the theoretically expected gaped Dirac surface states in these time-reversal symmetry broken topological materials, the electronic band structures are variously reported with regard to the presence of the band gap in the Dirac cone. Here we report on Sb doped higher order Mn-Bi-Te magnetic topological materials with a combining study of magnetotransport and Angle-Resolved Photo Emission Spectroscopy (ARPES). We found a multiple magnetic ground state with the doping of Sb in the antiferromagnetic topological insulator $MnBi_4Te_7$ owing to a delicate magnetic interaction strength along its van der Walls interlayer direction. We see a gradual shift of Fermi level from conduction band to the valance band with the Sb doping through charge compensation at 33% of Sb doping. Most interestingly, we found a gapless Dirac states in the pristine $MnBi_4Te_7$ and a gapped states in the Sb-doped $MnBi_4Te_7$. We discuss such unconventional scenario with the light of recent study from various research groups.

* sangc@physics.rutgers.edu

I. INTRODUCTION

The coexistence of long-range magnetic order and topological electronic states in a single phase material so called Magnetic topological insulator(TI)/conductor has become an exiting subject of study due to their emergent quantum phenomena such as quantum anomalous hall effect (QAH), topological magnetoelectric/Hall effect in axion insulator state, proximity effect, Weyl semimetals in layered van der Walls materials, potential for dissipationless spintronic applications [**?** **?** **?** **?** **?** **?** **?** **?**]. Many challenging issues in this field inspired a rapid theoretical and experimental research such as QAH effect arising from the chiral edge states that exists even under zero magnetic fields was experimentally observed in the ferromagnetically doped TI thin films e.g. $Cr_x(Bi_{0.1}Sb_{0.9})_{2-x}Te_3$ at very low temperature (<1 K) [**?** **?**]. In the axion insulator phase, one can observe a high longitudinal resistance and thereby a topological magnetoelectric effect involving a specific magnetic arrangement in accordance with the topological band crossing [**?**]. Unlike the inhomogeneous doped materials, the stoichiometric materials are expected to have such quantum phenomena at higher temperatures with more shophisticated tunability [**?** **?**].

Recently, natural van der Waals material namely $MnBi_2Te_4$ was recently grown as bulk crysals as well as thin film where QAH effect and axionic insulating state was demonstrated through tuning the magnetic structure by applying magnetic field at much higher temperatures. The most remarkable nature of $MnBi_2Te_4$ is that it is composed of septuple layers combining a quituple layer of Bi_2Te_3 and a Mn-Te layer which allows one to make a various new materials in a series with the addition of number of quituple layers of Bi_2Te_3, such as $(MnBi_2Te_4)(Bi_2Te_3)n$ (n = 0, 1, 2, ...). $MnBi_2Te_4$ is a A-type antiferromagnetic Z2 topological insulator where the spins are alligned ferromagnetically in the ab plane and coupled antiferromagnetically along c-direction [**?** **?** **?** **?** **?**]. $MnBi_2Te_4$ is intrinsically n-type carrier doped where through a gating effect the Fermi lavel could be tuned to the charge neutrality therefore a zero field or magnetic field induced QAH effect was realized up to 6.5 K. Furthermore, experimentally observed magnetism induced band gap opening was much less than that was theoretically expected. Currently, there are several reports on Sb doped in $MnBi_2Te_4$ by magneto-transport and electronic structure study through Angle Resolved Photo Emission to address various aspects in the electronic properties as Sb could be a successful dopant without destroying the topological character in the material [**?** **?**

?]. On the other hand, $MnBi_4Te_7$ having similar magnetic ground state with a delicate interaction strength making it more promising for the study of its electronic properties. Yet there has been few studies on Sb doping in $MnBi_4Te_7$ where one can tune it from antiferromagnetic (AFM) to a ferromagnetic (FM) transitions owing to weak magnetic interaction [? ? ? ? ? ?]. It appears that 147 phase of crystals grow critically in a very narrow temperature window compared to the 124 phase particularly with Sb doping. Furthermore, while doping with the Sb, it is prone to a arguably anti-site disorder effect that dependents heavily on the growth recipe. In this article, we have shown high-quality crystal growth of Sb doped $Mn(Bi_{1-x}Sb_x)_4Te_7$ (x = 0, 0.26, 0.37, and 0.48) crystals . We found a multiple magnetic ground state including a FM with Sb-substitution of Bi. Furthermore, from the electronic transport study, we have demonstrated AHE below both AFM and FM ground states. From our Angle-Resolved Photo Emission Spectroscopy (ARPES), We found an unusual gapless surface state in the pristine $MnBi_4Te_7$ whereas a gaped surface state in the Sb doped $MnBi_4Te_7$ crystals which is in agreement with the recent ARPES study. From high resolution spin-resolved photo electron spectroscopy, we found an evidance of in-plane magnetic spin structure on the surface which explains the gapless state in $MnBi_4Te_7$.

II. EXPERIMENTS

Single crystal growth: The $Mn(Bi_{1-x}Sb_x)_4Te_7$ (x=0, 0.26, 0.37, and 0.48) single crystal were grown by a standard high-temperature self-flux technique. A mixture Bi_2Te_3 (Alfa Aesar, purity 99.999%) and Sb_2Te_3 (Alfa Aesar, purity 99.999%) in a required ratio have been used as flux. The over-all ratio of precursors MnTe (Alfa Aesar, purity 99.9%) and $(Bi/Sb)_2Te_3$ flux were taken in 1:6 molar ratio. The mixture was placed in an alumina crucible and covered with an alumina frit disc and another another empty crucible was kept facing down towards the frit disc. The whole crucible assembly were sealed in a quartz tube at 10^{-4} torr after three times purged with Ar (99.999%). The ampule was first heated up to 950 °C in 12 hrs and dwelt there for 10 hrs to obtain a homogeneous liquid. Subsequently, it was cooled down to a temperature slightly above the melting temperature of the mixture of Bi_2Te_3 and Sb_2Te_3 flux, i.e. in between 580 to 620 °C in 10 hrs and further soaked there for 24 hrs. Then the ampule was further slowly cooled down for 10 °C in 100 hrs for the growth of crystals. It was then kept there for 24 hrs for the annealing process. The ampule was then

quickly taken out from the furnace and decanted the excess fluxes by centrifuging. Since the flux melting temperature is only a little higher than the crystal melting temperature, centrifuge was done in a quick manner. The obtained crystals were in plate shape with a typical dimension of 3 × 3 × 0.5 mm^3. The crystal 147 phases were confirmed by the (0 0 L) X-ray diffraction (XRD) peaks at room temperature using Panalytical diffractometer. Since there is a chance of remaining $(Bi/Sb)_2Te_3$ phase in the crystal, a special care was taken while selecting the crystals. The energy dispersive spectroscopy performed in high resolution field emission scanning electron microscope (JSM 7800F PRIME with Dual EDS, Hitachi) confirms the stoichiometry of Mn, Bi,Sb and Te (Fig. 1) in each studied crystals. Magnetization was measured under magnetic field along the *ab*-plane and *c*-axis using Magnetic Property Measurement System (MPMS, Quantum Design). The in-plane resistivity and Hall effect was measured in the standard four probe configuration using a Physical Property Measurement System (PPMS-9T, Quantum Design).

ARPES: ARPES measurements on single crystals of $MnBi_4Te_7$ and Sb-doped $MnBi_4Te_7$ were carried out at the Laser-ARPES system at Hiroshima Synchrotron Orbital Radiation (HiSOR) and ($h\nu$ = 6.3 eV) and at the Institute for Solid State Physics (ISSP) ($h\nu$ = 6.3 eV). Single crystals were cleaved in-situ in an ultra-high vacuum better than 2x10^{-11} torr. ARPES spectra were taken at 40 K and 10 K above and below the N*é*el temperature.

III. RESULTS AND DISCUSSIONS

A. Structural characterization

Fig. 1a shows the layered rhombohedral structure consisting of $Mn(Bi/Sb)_2Te_4$ and a quintuple spacer layer of $(Bi/Sb)_2Te_3$ [**?** **?**]. The Fig. 1b shows the X-ray diffraction (XRD) patterns of the various Sb doped single crystals on (00L) plane where all the (00L) peaks can be indexed by the 147 phase. We noticed that all the (00L) peaks for the four different concentration of Sb are nearly overlapped. Since the crystals are grown by the $(Bi/Sb)_2Te_3$ fluxes and the centrifuge temperatures were very close to the melting point of the fluxes, it is quite possible that there is a secondary phase of $(Bi/Sb)_2Te_3$ remained in the crystals. If there is a significant $(Bi/Sb)_2Te_3$ impurity phase, a clear peak could be observed at 17.5 degree which is below (005) peak. The absence of a visible peak near 17.5 degree indicates that there is no $(Bi/Sb)_2Te_3$impurity phase. Further, in order to avoid any such

impurities, we carefully cut off the crystal boundaries before performing the various studies. The actual Sb concentration in the Bi site was obtained from the EDS analysis. We see a slightly higher composition of the Sb compared to the nominal composition aimed during the crystal growth. Here we only mention the actual composition of compounds derived from EDS analysis. The XRD peaks on (00L) planes of the Sb doping compounds of x=0.26, 0.37 and 0.48 show tiny shifts towards the higher side indicating a subtle decrease of the c-axis lattice parameter (Fig. 1b inset).

B. Magnetization and magnetotransport properties

Figure 2(a-d) and Figure 3(a-d) summarizes the temperature dependent DC magnetic susceptibilty measured along both ab plane and along the c-axis under Zero Field Cooled (ZFC) and Field Cooled (FC) conditions. As we learned in the previous report that pristine $MnBi_4Te_7$ undergoes an AFM transition at 13 K and a spin flop transition at 2000 Oe, we see a clear AFM transition at 13K with a spin flop transition at 2000 Oe establishing a high quality crystals in our study (Fig. 3). Our temperature dependent in-plane resistivity data also reveals the AFM transition showing a clear cusp at 13 K due to spin disorder scattering at the magnetic transition (Fig. 2a). The rapid decrease of the resistivity below T_N, is due to the suppression of the spin scattering with the magnetic ordering. For Sb doping with x=0.26, we see almost no change in the T_N, however most interestingly we observe another magnetic transition below 8 K, as clearly evidenced in the ZFC magnetization with a sudden increase of magnetization and a bifurcation in the ZFC and FC measured along the c-axis (Fig 2b). With the increasing of the Sb doping (x=0.37) we noticed a more clear and disguised peak at the low temperature at 5.5K in both ZFC as well as FC magnetization in addition to the AFM ordering at 13 K (Fig. 2c). Most interestingly, we also observe the distinct anomalies in the in-plane resistivity measurement which demonstrate a robust change in the spin ordering at low temperature (Fig 3c). For 48% of Sb doping, the new magnetic transition persists with a subtle change in the temperature. Thus, the low-temperature magnetic ordering in Sb doped $MnBi_4Te_7$ family clearly distinguishes it from its parent compound $MnBi_2Te_4$. This striking behavior makes this family of compounds more interesting in terms of the Anomalous hall effect as well as Dirac surface states being the magnetic transition as a the crucial parameter for magnetic topological candidates. In order to understand the type of magnetic ordering, we measured field-dependent magnetization at different temperatures. The low-temperature M(H) data shows a ferromagnetic loop

with a very tiny coercive field indicating a ferromagnetic ground state below the second magnetic transition for all the Sb doped (x=0.26, 0.37 and x=0.48) compounds. On the other hand, in the $MnBi_4Te_7$, we see a spin-flip transition from AFM to a FM at 2000 Oe field. At the intermediate temperature, for x=0.37 and 0.48 compounds, we see a similar spin-flip AFM to FM transition at a lower coercive field of 1500 Oe and 500 Oe respectively. Therefore, here we suggest that the second magnetic transition is ferromagnetic in nature while the high temperature is an AFM transition similar to the $MnBi_4Te_7$. The origin of the second magnetic transition is presumed to be due to the presence of Mn antisite disorder as mentioned recently an almost unavoidable scenario [**?** **?**]. Previous studies on MnBi2Te4 and MnSb2Te4 have revealed the antisite disorder and mixing of Mn and Bi ions [**?**]. This is because of the intermediate bonding of Mn in the Bi_2Te_3 layer before they form a separate atomic layer [**?** **?**]. A glassy phase of magnetic ordering has also been reported in the Sb-doped $MnBi_4Te_7$ due to the Mn site mixing which explains the bifurcation of the ZFC and Fc magnetization [**?**]. However, single-crystal neutron diffraction measurements are needed for the detailed study of the site disorder and the magnetic ordering.

Now we discuss the magnetotransport behavior in $Mn(Bi_{1-x}Sb_x)_4Te_7$. Figure 3 (e-h) shows the in-plane longitudinal magnetoresistance for x=0, 026, 0.37 and 0.48 respectively at low field regime where we show the M(H) curve on the top panels. In the pristine sample, We observe a hysteric behavior at low field corresponding to the spin-flip transition and it diminishes with the increasing of temperature. The overall negative magnetoresistance (MR) can be due to the gradual suppression of the spin disorders with the magnetic field which is maximized near the magnetic ordering temperature. The sudden jump of the MR at spin-flip transition is due to the change in the spin orientations. With the doping of Sb=0.26, a overall positive MR was observed in contrast to the other doping level of the Sb (0.37 and 0.48). The origin of positive MR can be due to a nearly compensating electron and hole concentration as observed in the 124 compound. For x=0.37, we see an overall negative MR with a maximum near 7 K, in the vicinity of the second magnetic transition. This suggests that the second magnetic transition is quite significant in 0.37 sample as we noticed in our magnetization data with a very distinct and sharp anomaly. For x=0.48, we see a similar negative MR maximum at the high-temperature AFM transition. This clearly suggests that with the Sb doping, there is a gradual appearance of the second magnetic transition that approaches to the high temperature AFM ordering with the higher doping

level. The magnetoresistance behavior for up to 3 T field is shown in Fig. 3(i-l) where we observe an unsaturated magnetoresistance due to the presence of the spin-orbit coupling.

C. Anomalous Hall Effect

The most distinctive observation in a magnetic topological compounds is Anomalous Hall Effect (AHE). Figure 4(a-d) shows the magnetic field variation of the transverse (xy) magnetoresistance, called as Hall Effect. In all of the samples, we see an anomalous Hall signature at the low field regime concomitant with the magnetization. In the pristine sample (x=0), we see a step-like behavior at 2000 Oe corresponding to the spin-flip transition. For the Sb-doped samples, we see a ferromagnetic type signature in the Hall resistivity which is a clear indication of the ferromagnetic behavior at the low temperature and consistent with the magnetization behavior as shown in Fig3(a-d). Importantly, the anomalous Hall contribution is increased with the increase in the amount of Sb doping, which is an indication of the ferromagnetic nature enhanced with the Sb doping. From the high-field data up to 3 T, we can see a significant Hall contribution present in all the compounds. The most striking observation is the change in Hall resistivity from negative to positive with Sb doping from x = 0.26 to x = 0.37, which implies the change in the carrier types from n-type to p-type. Using $n{=}H/e\rho_{xy}$, the carrier concentration has been calculated from the Hall resistivity at 50 K as 1.8, 4.7, 0.2 and 0.9 X10^{20} cm^{-3} for the pristine and x=0.26, 0.37 and 0.48 respectively, similar to that of $MnBi_2Te_4$ [**?**].

D. Topological surface states

Bulk $MnBi_4Te_7$ has been established as a topological insulator through ARPES measurements by several groups[**?** **?** **?**]. The electronic band structure and the variation of Fermi level for x=0, x=0.26 and x=0.48 observed at the $MnBi_2Te_4$ surface termination in our ARPES experiments are shown in Fig. 5. We can clearly see the presence of tolological surface states on the top of the valance band for the pristine and x=0.26 doped compounds indicating the electron doping in contrast with the tails of the lower Dirac cone, visible near the Fermi level in the case of x=0.48 indicating significant hole doping so that the Dirac point is far above the Fermi level. A projection of the shifting of the Dirac point is shown with the dashed arrow. Perhaps the most arguable observation is the absence of a band gap in the Dirac cone in the electronic band structure of $MnBi_4Te_7$ [**?** **?** **?**]. In the case of $MnBi_2Te_4$, a gapless surfaces state was explained through the preservation of a combined symmetry ($S^{1/2}$) of time reversal (S) and half-lattice translation (1/2) along the c-axis [**?** **?**

?]. However, in case of $MnBi_4Te_7$, the combined symmetry does not exist and the magnetic configuration is A-type, which allows an open gap in the dirac cone and indeed there are some report showing gapped surface states in $MnBi_4Te_7$ [**?** **?**]. However, there are some groups which reported a gapless surface states [**?** **?**]. Thus, it is an open question whether the pristine $MnBi_4Te_7$ is truly gapless? Our ARPES measurement with 6.3eV Laser on the pristine $MnBi_4Te_7$ suggests a gapless states. Furthermore, a gapped surface state of about 75 meV is observed in the Sb doped compound (x=0.26) at 10 K (Fig. 6). We argue that for the pristine $MnBi_4Te_7$ case, there is in-plane Mn-spins which leaves the gapless surface states, whereas in the case of Sb-doping, a ferromagnetic interaction is more dominant which allows to extend the surface states into more septuple layeres thus showing a gapped state. Returning to reports that show a gapped surface state in the pristine $MnBi_4Te_7$, we argue that it most likely depends on the sample synthesis condition. During the crystal growth, slow cooling from higher temperature could allow more Bi and Mn site mixing that favor a ferromagnetic interaction and showing the gapped states as in the case of doped samples. In our case, the sample was rapidly cooled down to just above the melting temperature of the desired phase followed by slow cooling which decreases the site mixing of Bi and Mn leaving a gapless state. A detailed experiment with the spin-resolved photoemission experiment is necessary to prove the surface in-plane spin arrangement.

Conclusions

In conclusion, we have successfully grown the single crystals and studied the magnetic and magnetotransport properties of pristine and Sb doped magnetic topological Insulator $MnBi_4Te_7$. A strong Antiferromagnetic transition is commonly observed in all the 147 compounds and a distinguished ferromagnetic-like ordering below 6 K is observed with the Sb-doping. The ferromagnetic character is more pronounced with the doping above 26 %. We have shown that the critical field of magnetic field induced AFM to FM transition decreases with the Sb doping signifying the favourable FM-like behavior. A cross-over from n-type to p-type carrier is observed with the Sb doping above 30 % from both the transport and ARPES measurements. We have clearly resolved a gapless surface states for the pristine $MnBi_4Te_7$ and a gapped (75 meV) surface state for the Sb-doped $MnBi_4Te_7$ sample with the help of a Laser-ARPES of phonon energy 6.3 eV.

Acknowledgement:

This work was supported by the Institute for Basic Science (IBS) through the Center for Artificial Low Dimensional Electronic Systems and W. M. Keck foundation grant to the Keck Center for Quantum Magnetism at Rutgers University.

Competing financial interests:

The authors declare no competing financial interests.

Additional information:

Correspondence and requests for materials should be addressed to Chandan De (email:).

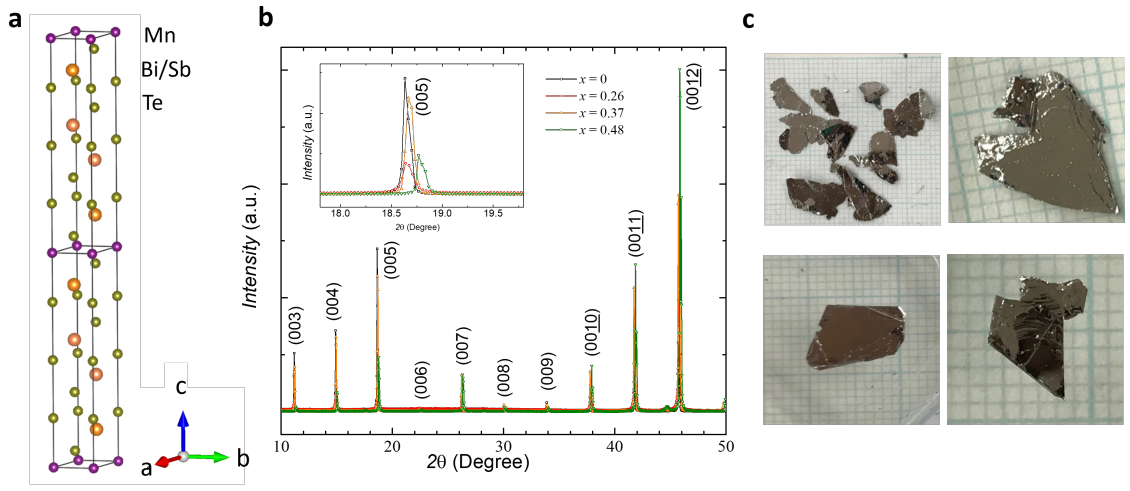

FIG. 1. (a) The Schematic Crystal structure of layered $MnBi_4Te_7$ with Sb doping at the Bi-site. Purple and Orange spheres represent the Mn and Te atoms respectively whereas the orange sphere represents the Bi or the Sb atoms. (b) The room temperature powder X-ray diffraction peaks from the ab plane of $Mn(Bi_{1-x}Sb_x)_4Te_7$ (x=0, 0.26, 0.37, 0.48) crystals. Inset shows the magnified peak of the (005) plane. (c) Image of the typical single crystals grown in this work

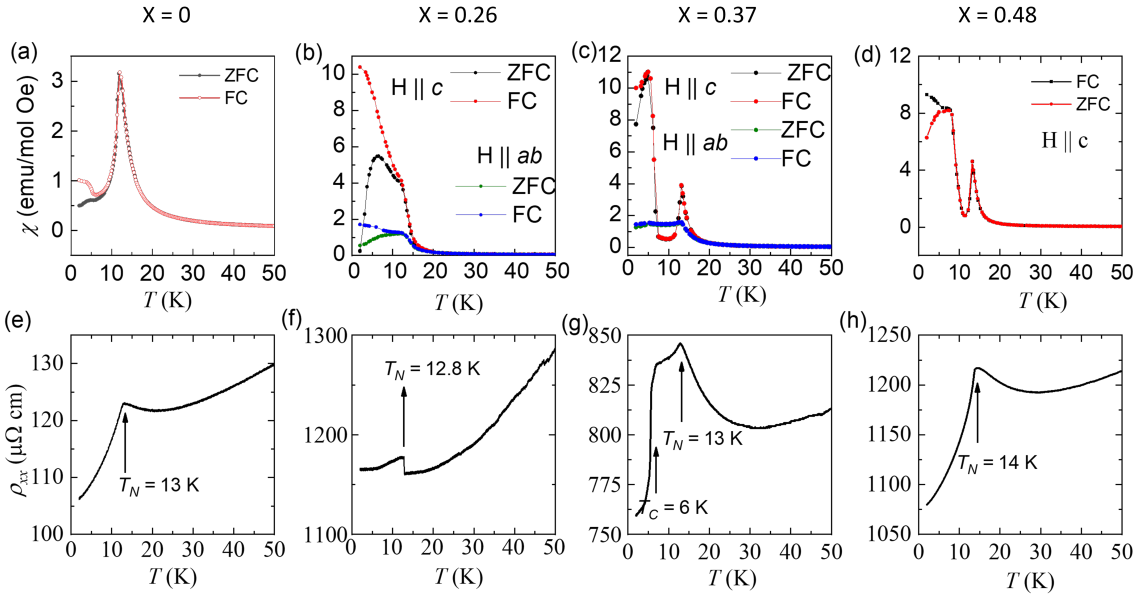

FIG. 2. (a-d) The temperature dependence of susceptibility (χ) under μ_0H = 0.01 T for H ∥ c and H ∥ ab plane for Zero Field Cooled and Field Cooled condition for the sample x= 0, 0.26, 0.37 and 0.48 respectively. (e-h) The temperature dependence of longitudinal resistivity (ρ_{xx}) at μ_0H = 0 T measured from 2 K to 50 K for the sample x= 0, 0.26, 0.37 and 0.48 respectively.

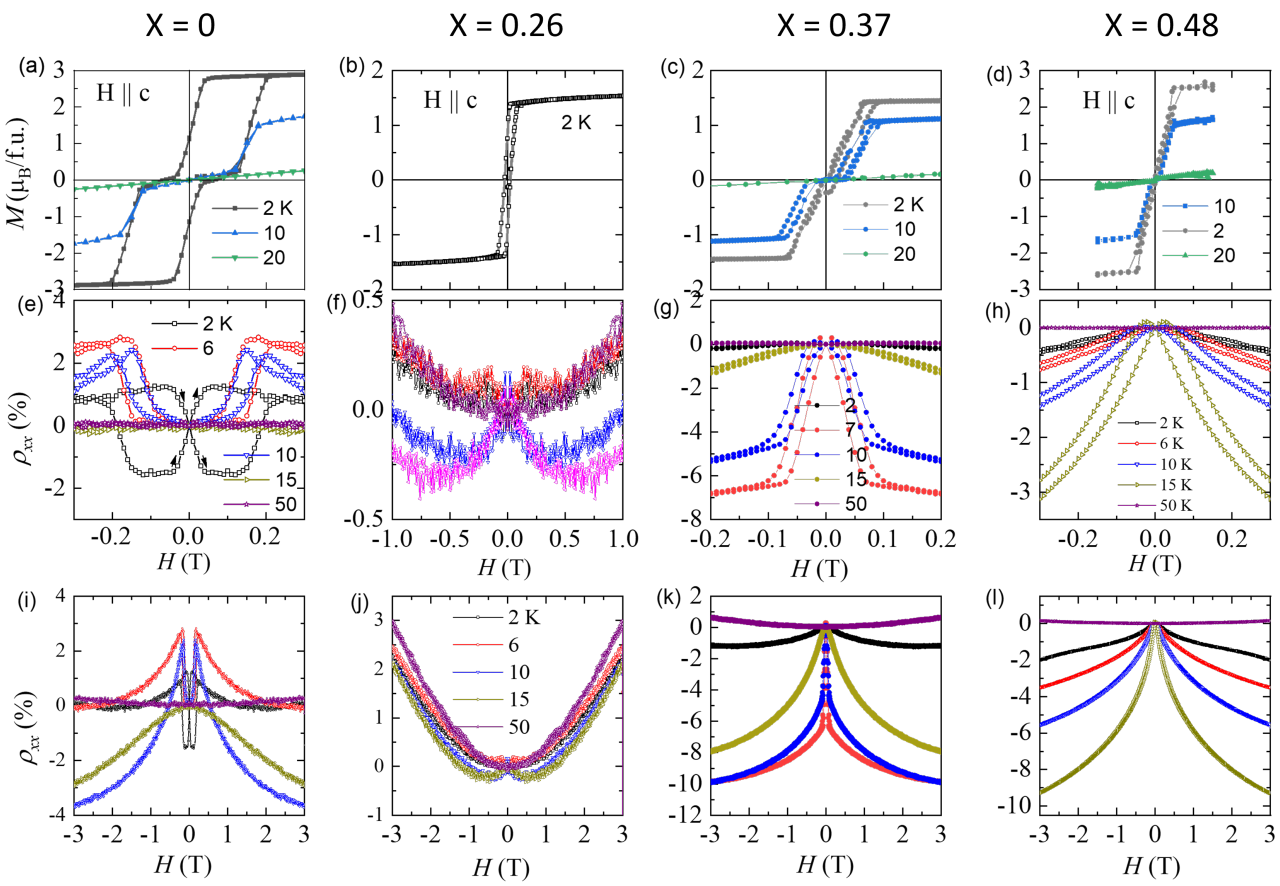

FIG. 3. Magnetization and Magnetotransport properties of bulk $Mn(Bi_{1-x}Sb_x)_4Te_7$ single crystal. (a-d) The magetic field (H) dependent Magnetization (M) under H ∥ c at various temperatures for the sample x= 0, 0.26, 0.37 and 0.48 respectively. (e-h) Longitudinal magnetoresistance (ρ_{xx}) on the ab plane I ∥ ab and H ∥ c at various temperatures under low magnetic field range up to 1 T for the sample x= 0, 0.26, 0.37 and 0.48 respectively. (i-l) Similar magnetoresistance data measured up to 3 T.

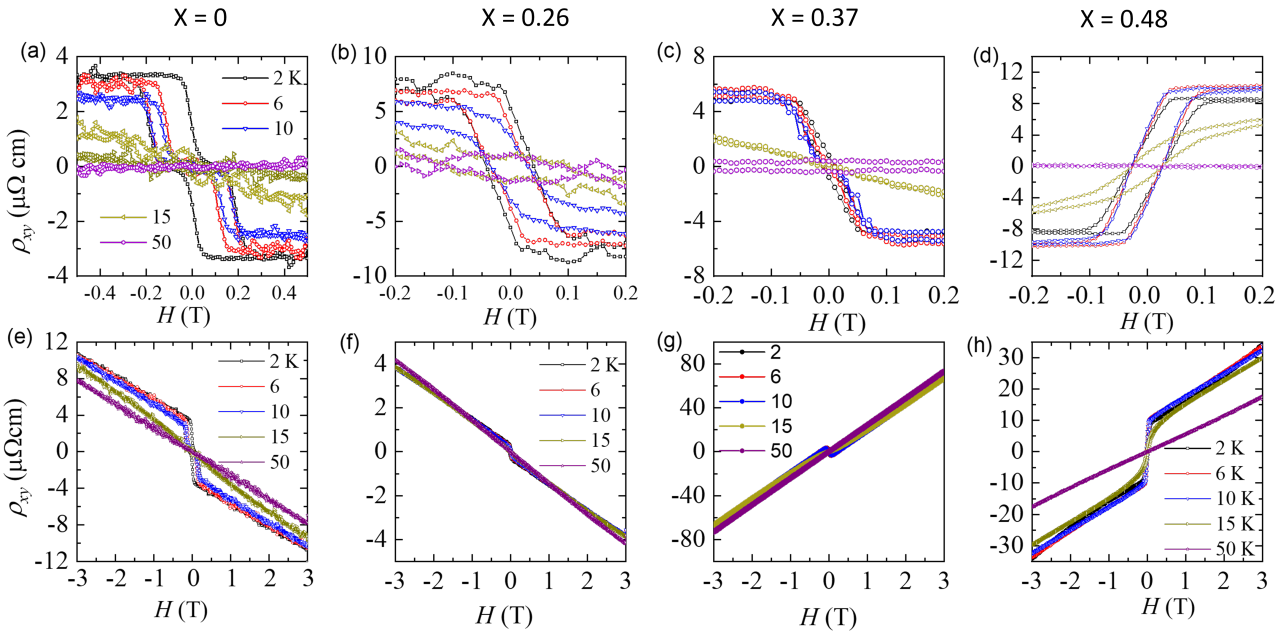

FIG. 4. The anomalous hall resistivity. (a-d) Anomalous Hall resistivity ($\rho_{xy}{}^{A}$) measured under a low magnetic field range after antisymmetrizing and subtracting the linear contribution to the transverse resistivity for the sample x= 0, 0.26, 0.37 and 0.48 respectively at various temperatures. (e-h) Transverse resistivity data measured up to 3 T for the same samples.

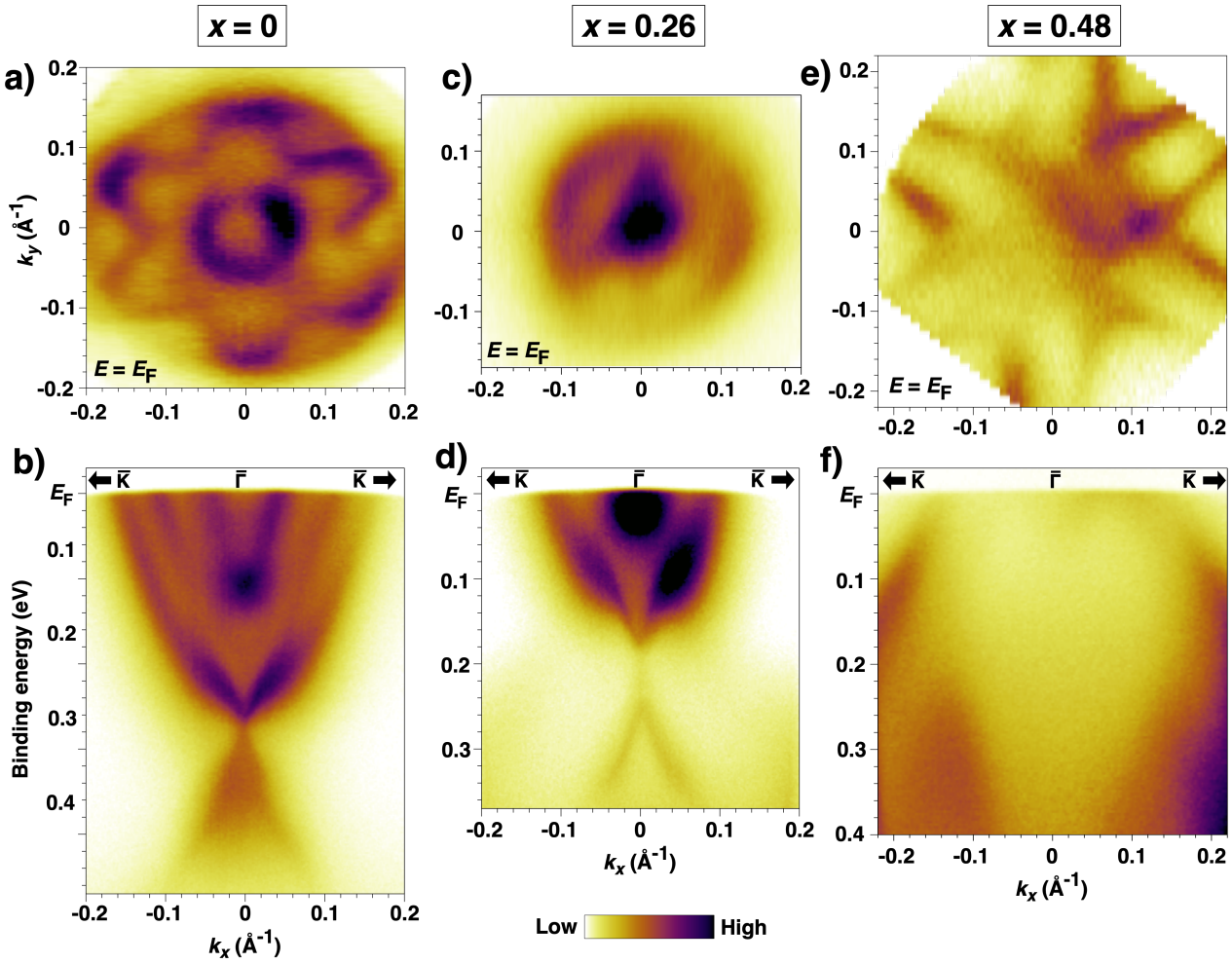

FIG. 5. ARPES intensity plot along the $\overline{\Gamma}$-$\overline{K}$ direction measured with $h\nu$ = 7.0 eV at 10 K for the sample x= 0, 0.26 and 0.48.

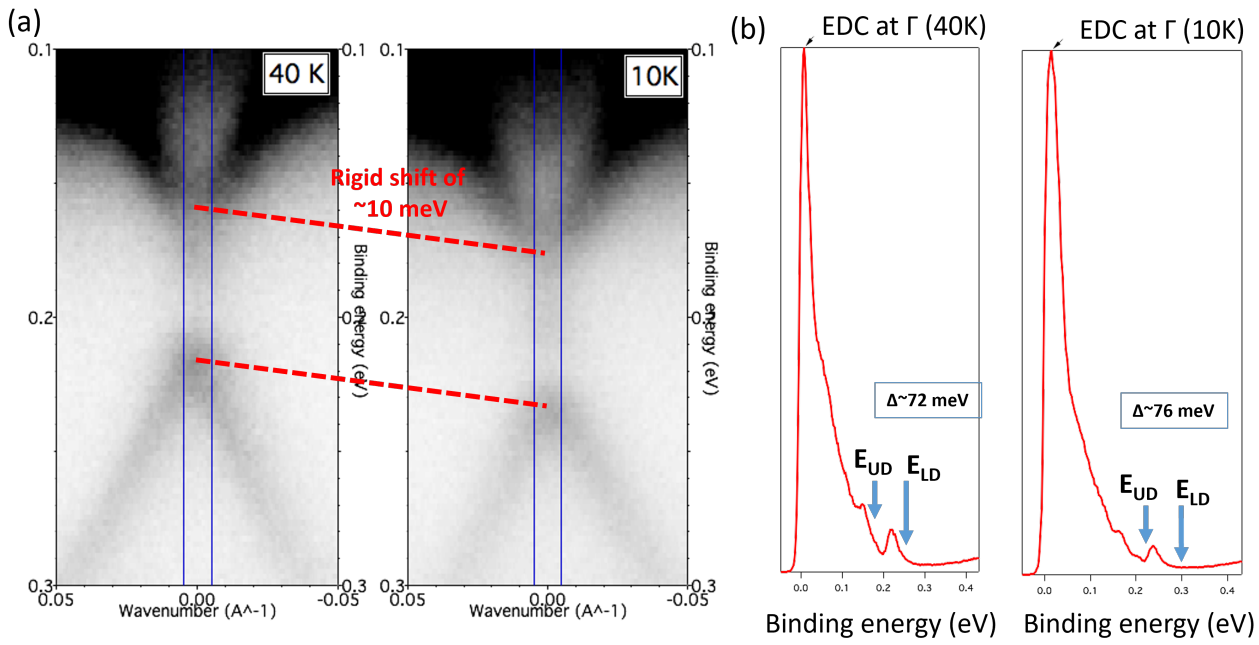

FIG. 6. ARPES data for the x=0.26 sample near the Dirac band (a) ARPES intensity plot along the $\overline{\Gamma}$-$\overline{K}$ direction measured with photon energy $h\nu = 7.0$ eV at 40 K (left) and 10 K (right). (b) Energy Distribution Curves (EDCs) at $\overline{\Gamma}$ for 40 K (left) and 10 K (right) showing the Upper-Dirac energy ($E_U D$) and Lower-Dirac energy ($E_L D$) peaks with gap opening $\Delta \approx 72$ mev and 76 mev at 40 K and 10 K respectively.